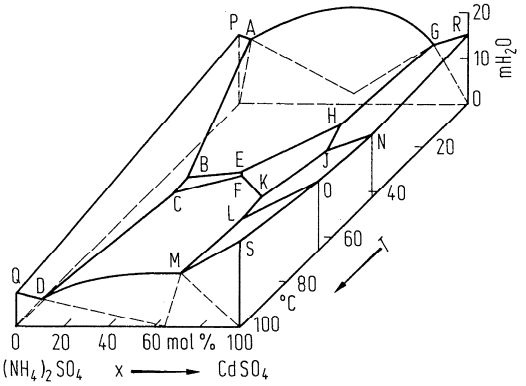

Fig. 43A-13-001. $(NH_4)_2Cd_2(SO_4)_3$. Phase diagram of $(NH_4)_2SO_4$–$CdSO_4$–H_2O system [32Ben]. The surface CDMLKF is a crystallization surface for $(NH_4)_2Cd_2(SO_4)_3$. x: concentration of $CdSO_4$.

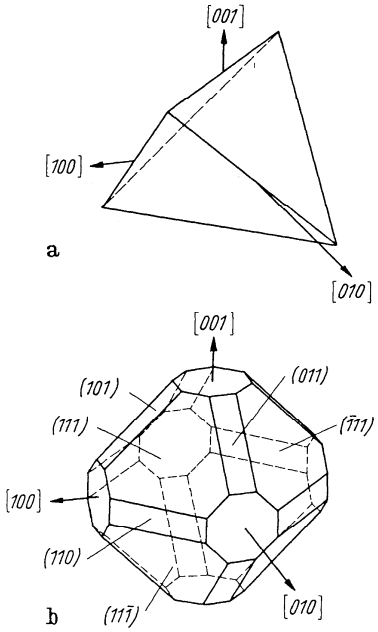

Fig. 43A-13-002. $(NH_4)_2Cd_2(SO_4)_3$. Crystal forms [57Eas]. (**a**) tetrahedral form; (**b**) cubic octahedral dodecahedral form.

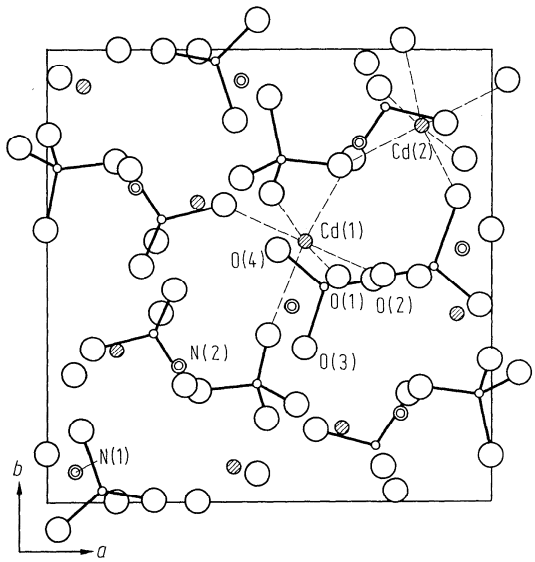

Fig. 43A-13-003. $(NH_4)_2Cd_2(SO_4)_3$. Crystal structure [75NgH]. (001) projection.

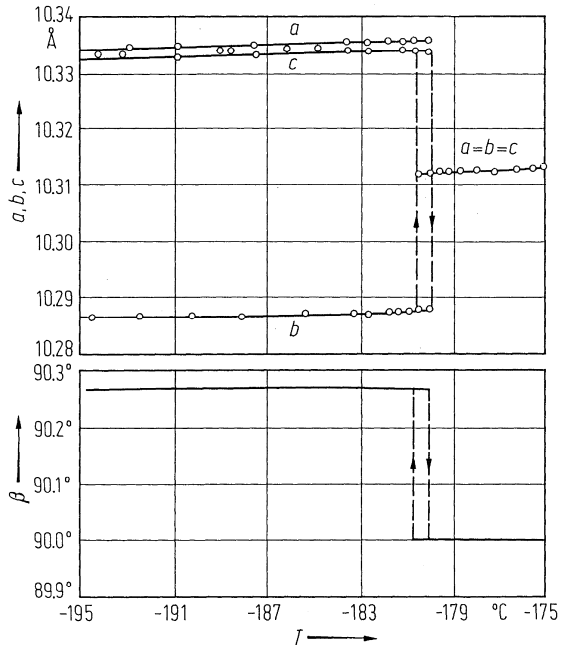

Fig. 43A-13-004. $(NH_4)_2Cd_2(SO_4)_3$. Unit cell parameters vs. T [78Kob].

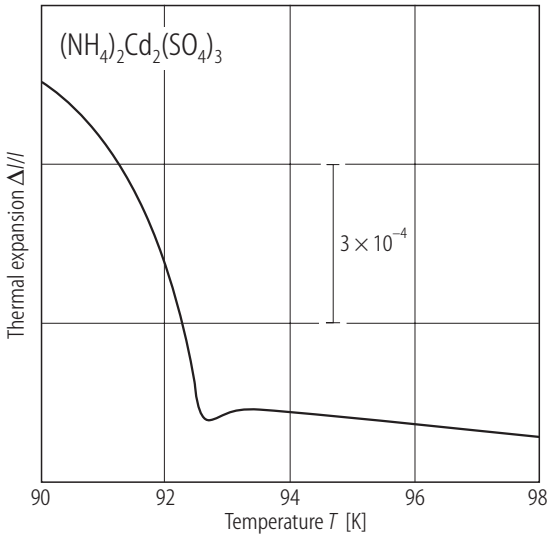

Fig. 43A-13-005. $(NH_4)_2Cd_2(SO_4)_3$. $\Delta l/l$ vs. T [88Kah]. $\Delta l/l$: fractional thermal expansion along the ⟨100⟩ axis. Relative to the brass dilatometer cell.

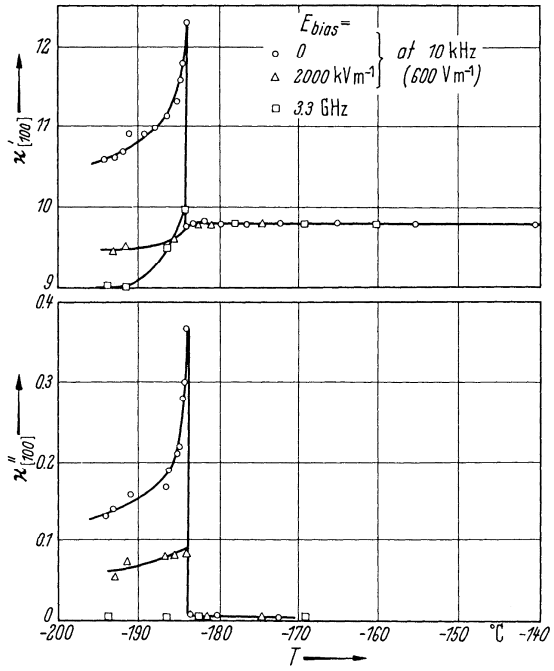

Fig. 43A-13-006. $(NH_4)_2Cd_2(SO_4)_3$. $\kappa'_{[100]}$ and $\kappa''_{[100]}$ vs. T [66Ohs]. $\kappa'_{[100]}$, $\kappa''_{[100]}$: real and imaginary parts of $\kappa_{[100]}$.

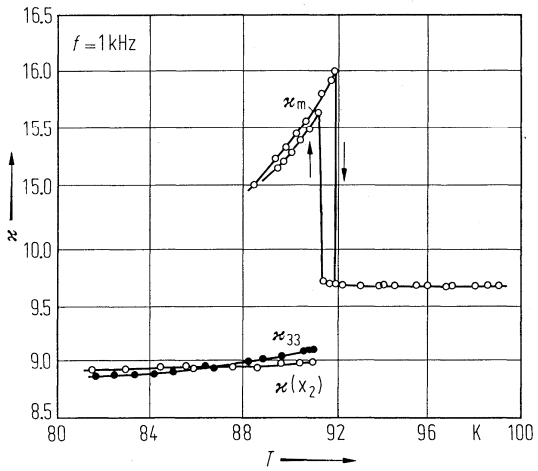

Fig. 43A-13-007. $(NH_4)_2Cd_2(SO_4)_3$. κ_{33}, κ_m and $\kappa(x_2)$ vs. T [73Glo]. κ_{33}: dielectric constant along the P_s of single domain crystal; κ_m: that of multidomain crystal; $\kappa(x_2)$: that with field perpendicular to P_s of x_2-domain crystal.

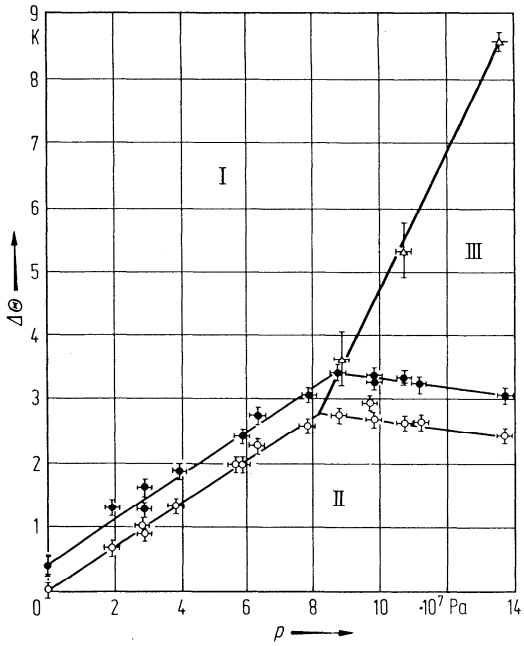

Fig. 43A-13-008. $(NH_4)_2Cd_2(SO_4)_3$. $\Delta\Theta$ vs. p [72Glo2]. $\Delta\Theta = \Theta(p) - \Theta_f(0)$. $\Theta_f(0)$: ferroelectric transition temperature at zero pressure. Full circles: on heating; open circles: on cooling.

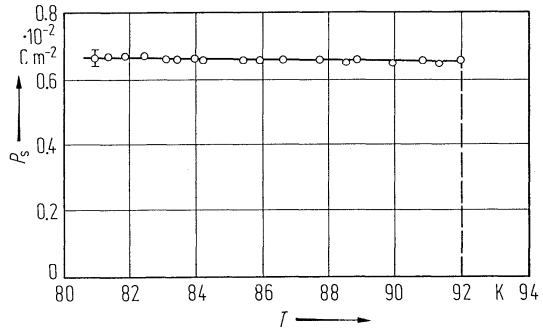

Fig. 43A-13-009. $(NH_4)_2Cd_2(SO_4)_3$. P_s vs. T [73Glo].

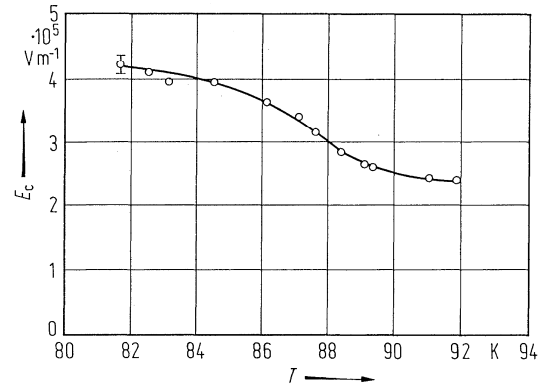

Fig. 43A-13-010. $(NH_4)_2Cd_2(SO_4)_3$. E_c vs. T [73Glo].

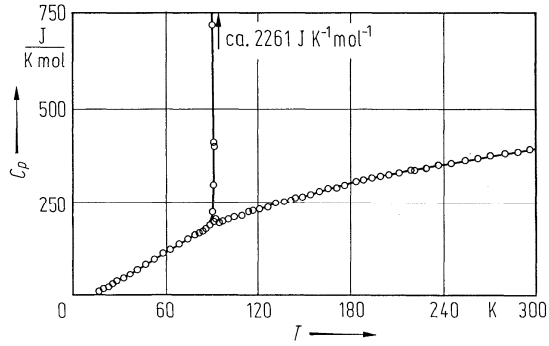

Fig. 43A-13-011. $(NH_4)_2Cd_2(SO_4)_3$. C_p vs. T [62Ste]. C_p: molar heat capacity at constant pressure.

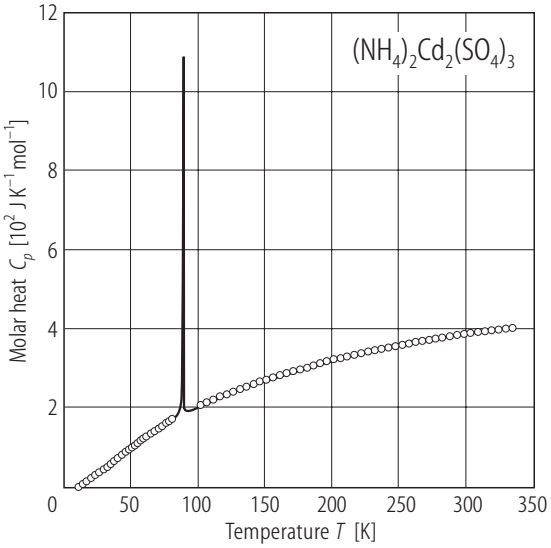

Fig. 43A-13-012. $(NH_4)_2Cd_2(SO_4)_3$. C_p vs. T [92Art]. C_p: molar heat capacity at constant pressure. The solid line represents the smoothed curve through the data points.

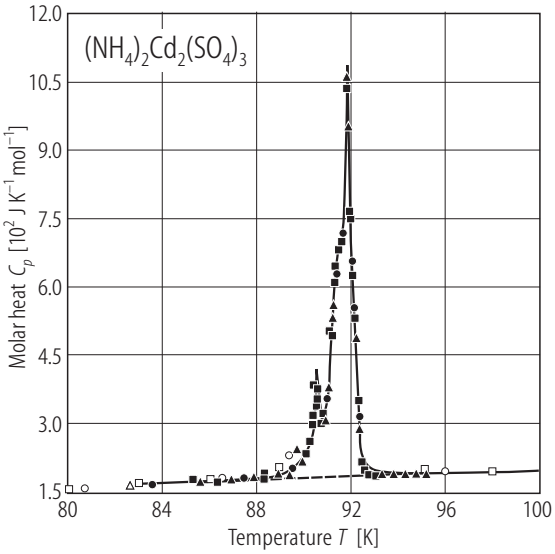

Fig. 43A-13-013. $(NH_4)_2Cd_2(SO_4)_3$. C_p vs. T [92Art]. C_p: molar heat capacity at constant pressure. An enlarged view illustrating the details of the transition region. The solid line represents the smoothed curve through the data points. The different symbols correspond to data from different series.

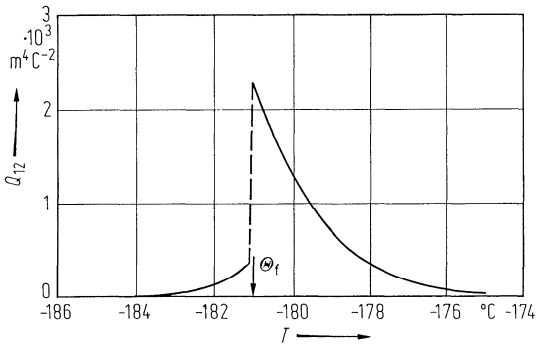

Fig. 43A-13-014. $(NH_4)_2Cd_2(SO_4)_3$. Q_{12} vs. T [62Ste]. Q_{12}: electrostrictive constant.

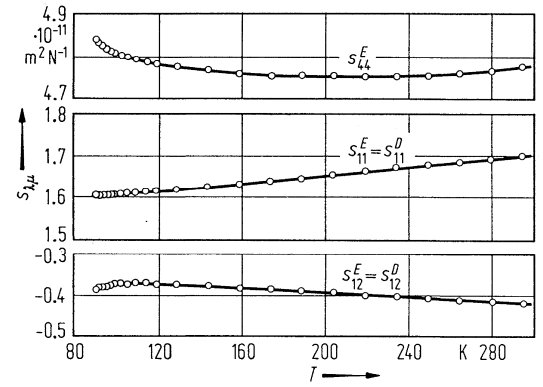

Fig. 43A-13-015. $(NH_4)_2Cd_2(SO_4)_3$. $s^E_{\lambda\mu}$, $s^D_{\lambda\mu}$ vs. T [72Glo1].

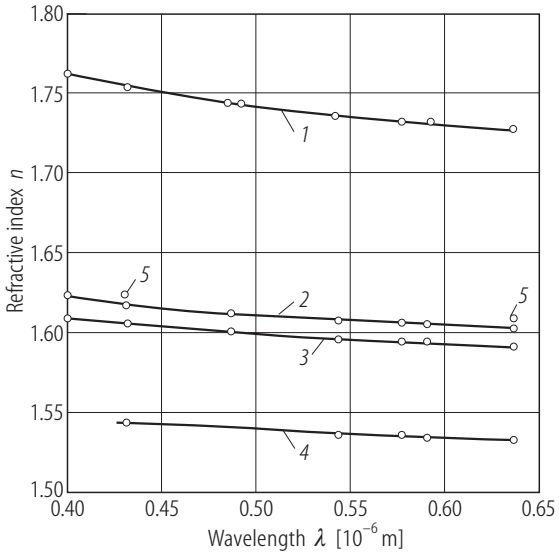

Fig. 43A-13-016. $(NH_4)_2Cd_2(SO_4)_3$ (*1*), $Tl_2Cd_2(SO_4)_3$ (*2*), $Rb_2Cd_2(SO_4)_3$ (*3*), $K_2Mg_2(SO_4)_3$ (*4*), $K_2Co_2(SO_4)_3$ (*5*). n vs. λ [87Bat].

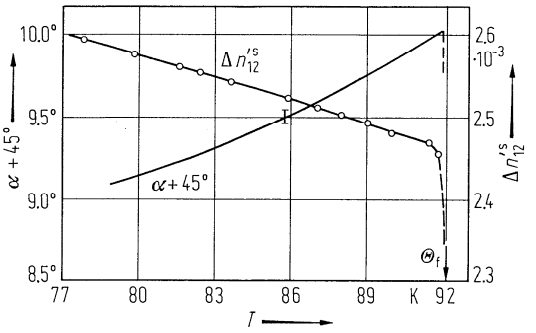

Fig. 43A-13-017. $(NH_4)_2Cd_2(SO_4)_3$. $\Delta n'^s_{12}$ and $\alpha + 45°$ vs. T [74Kon]. $\Delta n'^s_{12}$: spontaneous birefringence, $\alpha + 45°$: spontaneous rotation angle. $\lambda = 633$ nm.

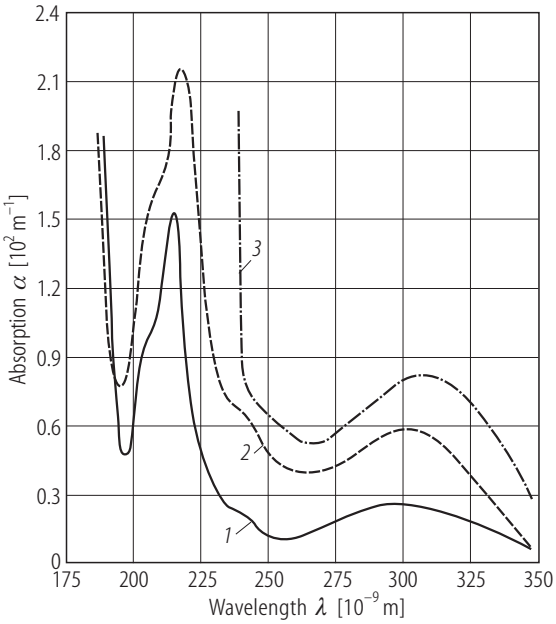

Fig. 43A-13-018. $(NH_4)_2Cd_2(SO_4)_3$, $Rb_2Cd_2(SO_4)_3$, $Tl_2Cd_2(SO_4)_3$. α vs. λ [89Bat]. α: absorption coefficient. (*1*) $(NH_4)_2Cd_2(SO_4)_3$ at 100 K; (*2*) $Rb_2Cd_2(SO_4)_3$ at 130 K; (*3*) $Tl_2Cd_2(SO_4)_3$ at 130 K.

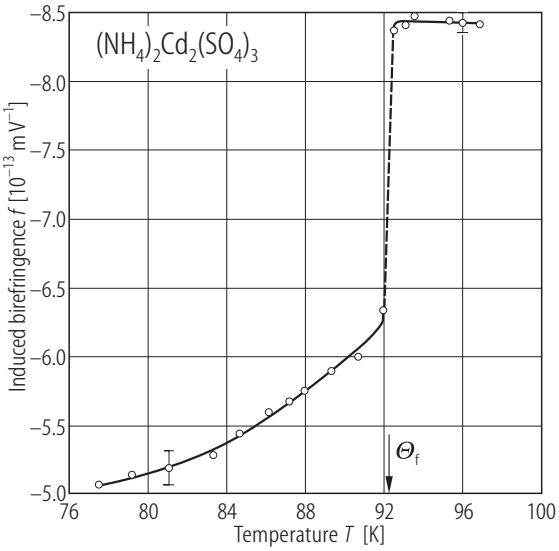

Fig. 43A-13-019. $(NH_4)_2Cd_2(SO_4)_3$. f vs. T [74Kon]. $f = (1/n_0^3)\cdot(d\Delta n'_{12}/dE_3)$ (induced birefringence).

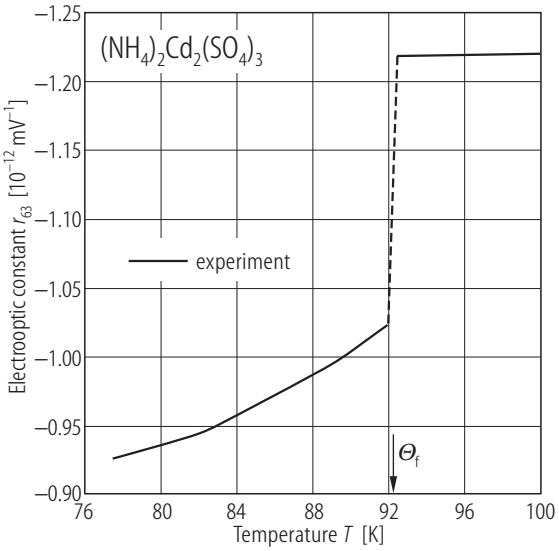

Fig. 43A-13-020. $(NH_4)_2Cd_2(SO_4)_3$. r_{63} vs. T [74Kon].

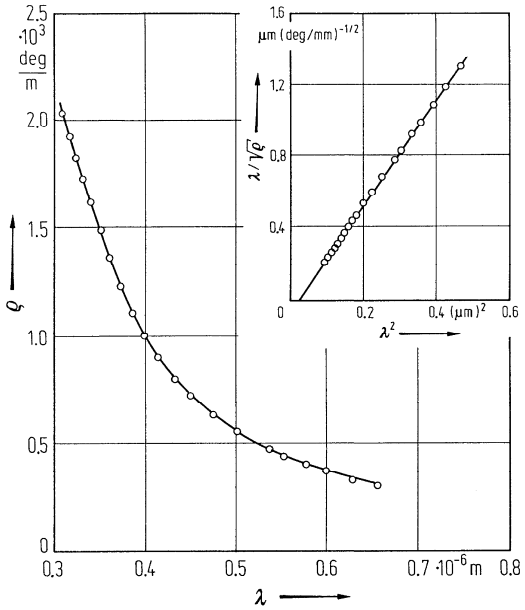

Fig. 43A-13-021. $(NH_4)_2Cd_2(SO_4)_3$. ρ vs. λ [74Iva]. ρ: optical rotatory power.

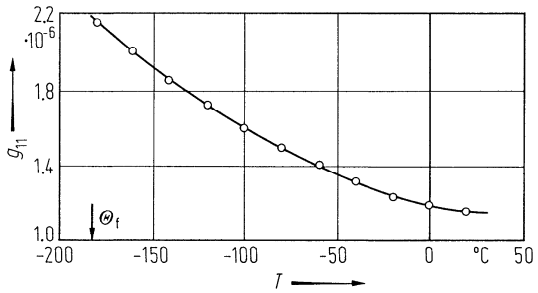

Fig. 43A-13-022. $(NH_4)_2Cd_2(SO_4)_3$. g_{11} vs. T [78Kob]. g_{11}: component of optical gyration tensor.

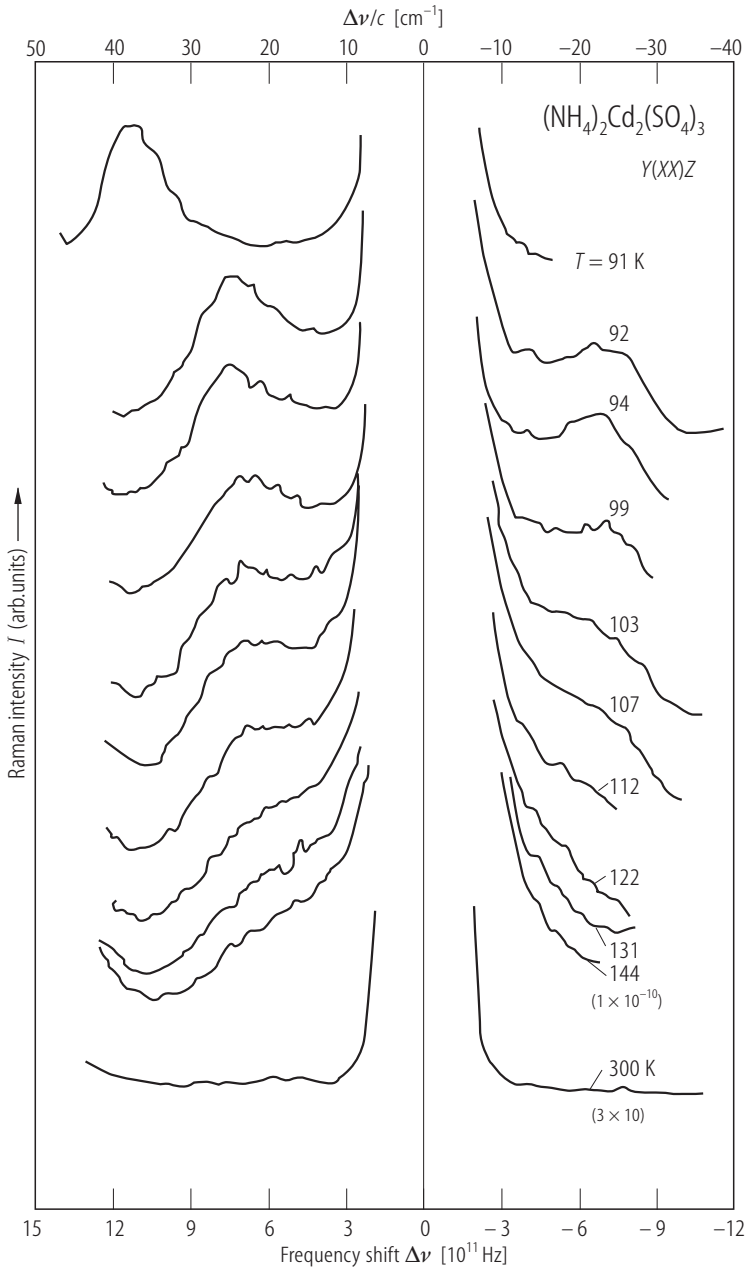

Fig. 43A-13-023. $(NH_4)_2Cd_2(SO_4)_3$. *I* vs. Δ*ν* [81Gal]. *I*: Raman intensity. Geometry: *Y*(*XX*)*Z*. Parameter: *T*.

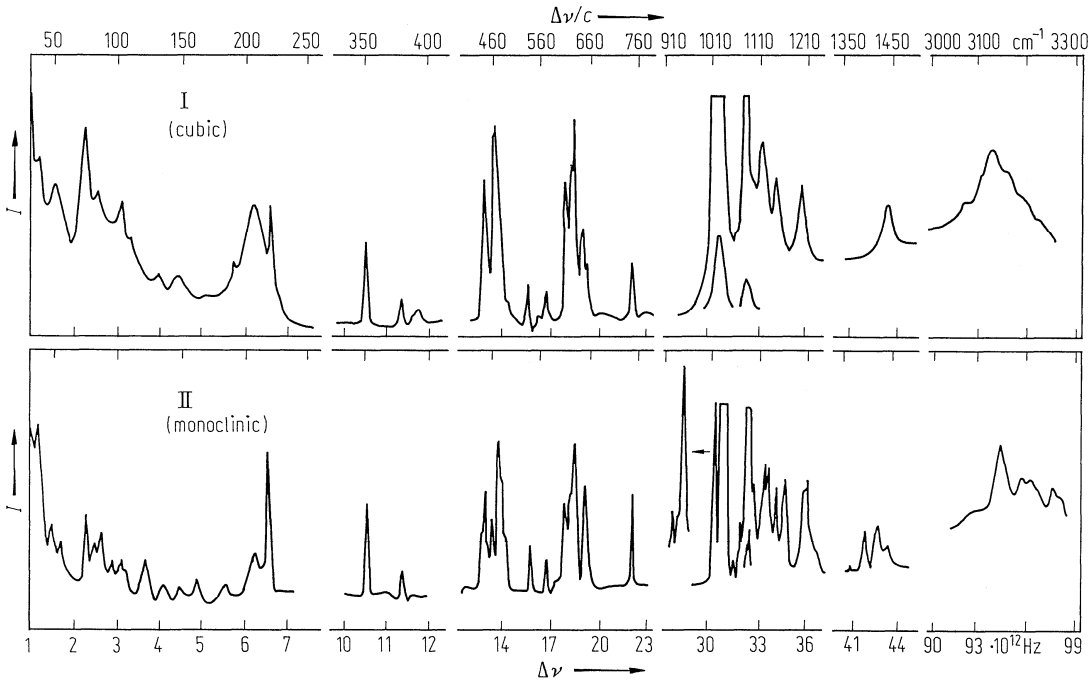

Fig. 43A-13-024. $(NH_4)_2Cd_2(SO_4)_3$. Depolarized Raman spectra in two phases [82Kre].

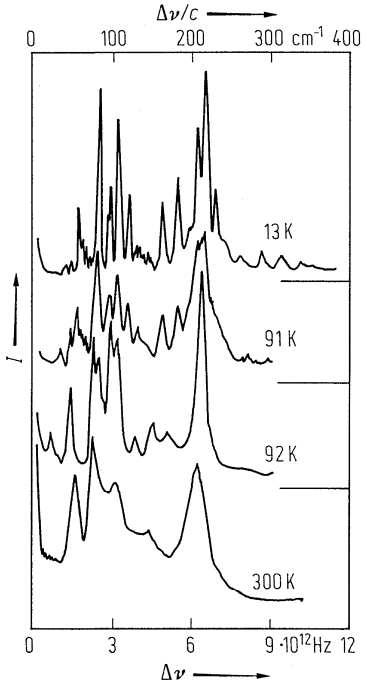

Fig. 43A-13-025. $(NH_4)_2Cd_2(SO_4)_3$. I vs. $\Delta\nu$ [78Gal]. I: Raman scattering intensity in the scattering geometry $Y(ZZ)X$. Parameter: T.

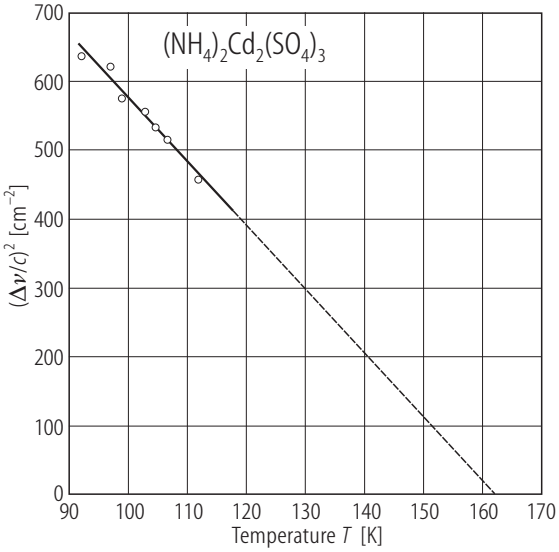

Fig. 43A-13-026. $(NH_4)_2Cd_2(SO_4)_3$. $(\Delta\nu/c)^2$ vs. T [88Gal]. Lowest optical Raman mode. An antidistortive phase transition is suggested at 162 K.

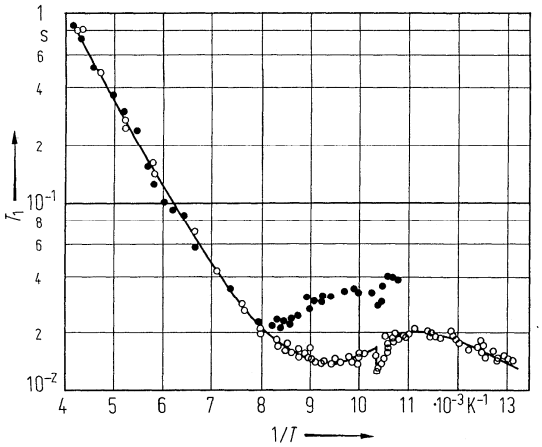

Fig. 43A-13-027. $(NH_4)_2Cd_2(SO_4)_3$. T_1 vs. $1/T$ [75McD]. T_1: proton spin-lattice relaxation time. Open circles: $f = 30.8$ MHz, full circles: $f = 48.2$ MHz.

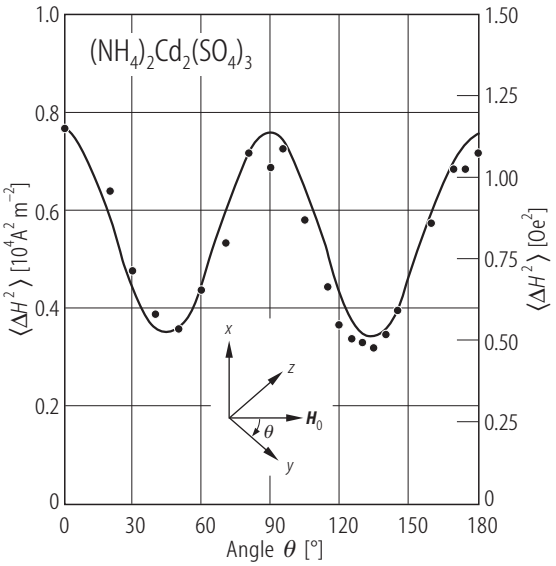

Fig. 43A-13-028. $(NH_4)_2Cd_2(SO_4)_3$. Proton second moment vs. θ [73Goc]. $\theta = \angle(y, H_0)$, H_0 being in the yz-plane.

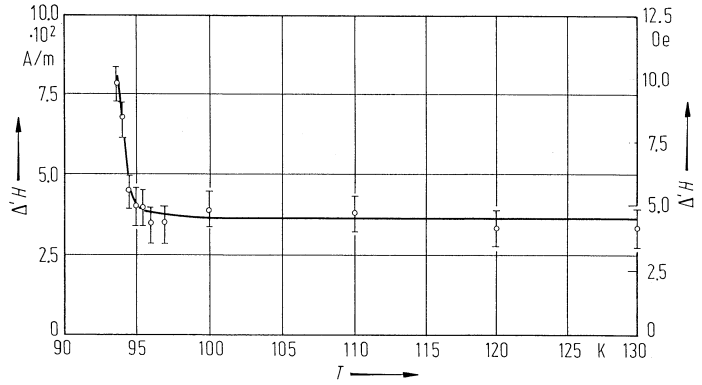

Fig. 43A-13-029. $(NH_4)_2Cd_2(SO_4)_3$. $\Delta'H$ vs. T [86Mis]. $\Delta'H$: linewidth of the highest-field Mn^{2+} ESR line. $H \parallel \langle 111 \rangle$.

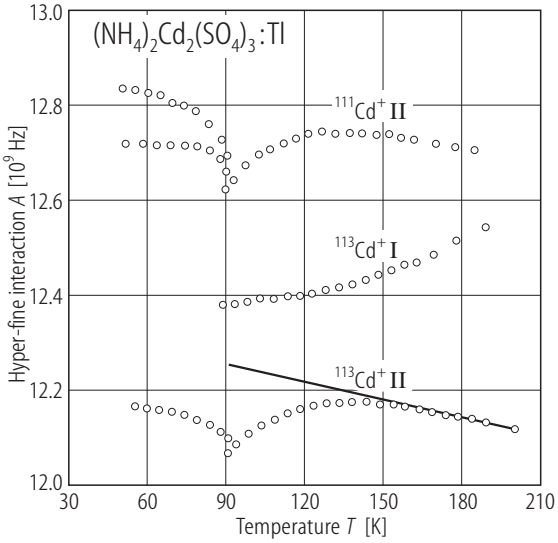

Fig. 43A-13-030. $(NH_4)_2Cd_2(SO_4)_3$:Tl. A vs. T [87Efi]. A: hyperfine interaction constant.

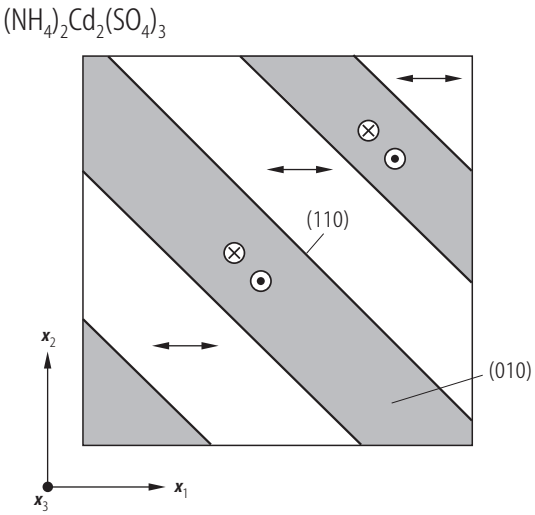

Fig. 43A-13-031. $(NH_4)_2Cd_2(SO_4)_3$. Typical domain pattern observed in an insulating (001) plate [73Glo].

$(NH_4)_2Cd_2(SO_4)_3$

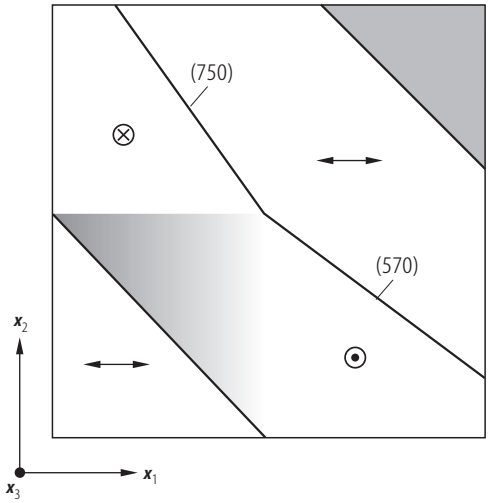

Fig. 43A-13-032. $(NH_4)_2Cd_2(SO_4)_3$. Typical domain pattern observed in a short circuited (001) plate [73Glo]. The angles of wedge shaped domains are exaggerated. Arrows indicate polarization directions.